15 May 2001

ELSEVIER

Optics Communications 192 (2001) 1–12

OPTICS COMMUNICATIONS

www.elsevier.com/locate/optcom

Non-paraxial beam propagation methods

P. Chamorro-Posada [a,*], G.S. McDonald [b,1], G.H.C. New [c,2]

[a] *Departamento de Teoría de la Señal, Comunicaciones e Ingeniería Telemática, E.T.S.I. Telecomunicación, Universidad de Valladolid, Campus Miguel Delibes, 47011 Valladolid, Spain*

[b] *Photonics and Non-linear Science Group, Joule Physics Laboratory, School of Sciences, University of Salford, Salford M5 4WT, UK*

[c] *Laser Optics and Spectroscopy Group, Blackett Laboratory, Imperial College of Science, Technology and Medicine, Prince Consort Road, London SW7 2BW, UK*

Received 5 December 2000; accepted 14 March 2001

Abstract

Exact analytical results are employed in the testing of split-step and finite difference approaches to the numerical solution of the non-paraxial non-linear Schrödinger equation. It is shown that conventional split-step schemes can lead to spurious oscillations in the solution and that fully finite difference descriptions may require prohibitive discretisation densities. Two new non-paraxial beam propagation methods, that overcome these difficulties, are reported. A modified split-step method and a difference-differential equation method are described and their predictions are validated using dispersion relations, an energy flow conservation relation and exact solutions. To conclude, results concerning 2D (transverse) beam self-focusing, for which no exact analytical solutions exist, are presented. © 2001 Published by Elsevier Science B.V.

PACS: 42.65.−k; 42.65.Jx; 42.65.Tg; 02.70.−c

Keywords: Non-linear optics; Self-focusing; Optical solitons; Computational techniques

1. Introduction

Spatial solitons are ideal candidates for binary elements in future optical information technology (IT) systems [1–11]. While soliton beams are usually solutions of paraxial wave equations, such as the non-linear Schrödinger equation (NSE), many important IT applications involve the breakdown of the paraxial approximation. Non-paraxiality may arise in the miniaturisation of devices and in other configurations, such as those involving multiplexed beams [12]. The non-paraxial non-linear Schrödinger equation (NNSE) has recently been shown to have exact analytical solutions [13] and general relations describing energy flow conservation and transformation invariance have also been derived [14]. Numerical studies are necessary to address key questions surrounding the stability and generation of solutions of such non-linear wave equations, but different algorithms for non-paraxial propagation problems have tended to yield distinct results [14–18].

* Corresponding author. Tel.: +34-983-423-000 ext.: 25545; fax: +34-983-423-667.

E-mail addresses: pedcha@tel.uva.es (P. Chamorro-Posada), g.s.mcdonald@salford.ac.uk (G.S. McDonald), g.new@ic.ac.uk (G.H.C. New).

[1] Tel.: +44-161-295-5079; fax: +44-161-295-5147.

[2] Tel.: +44-20-7594-7791; fax: +44-20-7594-7714.

0030-4018/01/$ - see front matter © 2001 Published by Elsevier Science B.V.
PII: S0030-4018(01)01171-3

Our exact analytical work has, for the first time, permitted the development and testing of existing and new non-paraxial beam propagation methods. Fundamental and higher order paraxial solitons have been found to be unstable in non-paraxial regimes [14]; launching of a fundamental paraxial soliton leads to re-shaping during propagation while higher order solitons tend to break up. This latter instability exhibits an intriguing bifurcation structure that appears to be of a general nature [14,19,20]. The corresponding analytical solutions of the NNSE exhibit solitonic robustness with respect to perturbations and act as attractors in non-linear beam evolution [14].

In this paper, we give a detailed account of two novel beam propagation methods that yield accurate results in non-paraxial regimes. A commonly used spectral approach [18] is shown to give rise to large deviations from the true solution; our first numerical method is a modified version of this scheme in which the progressive inclusion of new higher order terms removes this artifact. Our second non-paraxial algorithm has more general applicability and employs an explicit finite difference scheme in the longitudinal direction; high accuracy is also demonstrated. The goal of our investigations is to tackle the long-standing problem of understanding the interplay between finite beam effects and medium non-linearity in the presence of both transverse and longitudinal linear diffraction. We study the NNSE as this equation succinctly describes this interplay and because a series of analytical results are now available to test numerical solutions. This work provides a reliable framework for further work in which a variety of additional terms may be included in the non-paraxial wave equation, and their relative importance evaluated. Additional terms could, for example, be the result of considering cavity geometries [1–11], light polarisation [17], interfaces [21,22], or effects such as the induced diffraction that arises from the inclusion of a non-zero divergence term in the wave equation [23]. We conclude this paper by examining the role of a second transverse dimension in the NNSE for the case when a Gaussian beam is launched into a self-focusing Kerr medium.

2. Non-paraxial non-linear Schrödinger equation

The scalar field envelope $u(\xi,\zeta)$ of a continuous wave beam experiencing linear diffraction in one transverse dimension in a self-focusing Kerr medium evolves according to the NNSE [13]

$$\kappa\frac{\partial^2 u}{\partial\zeta^2}+\mathrm{i}\frac{\partial u}{\partial\zeta}+\frac{1}{2}\frac{\partial^2 u}{\partial\xi^2}+|u|^2u=0, \tag{1}$$

where ζ and ξ (z and x) are the scaled (unscaled) longitudinal and transverse coordinates respectively, and

$$\zeta=\frac{z}{L_{\mathrm{D}}},\quad \xi=\frac{\sqrt{2}x}{w_0},\quad u(\xi,\zeta)=\sqrt{\frac{kn_2L_{\mathrm{D}}}{n_0}}A(\xi,\zeta). \tag{2}$$

w_0 is a transverse scale parameter that can be considered as equivalent to the waist of a (reference) Gaussian beam with diffraction length $L_{\mathrm{D}}=kw_0^2/2$. $k=n_0\omega/c$, n_0 is the linear refractive index, n_2 is the Kerr coefficient, $A(\xi,\zeta)$ is unscaled field and $\kappa=1/(kw_0)^2=(\lambda/w_0)^2/4\pi^2n_0^2$, where λ is the optical wavelength. Eq. (1) quantifies changes in the transverse profile of a light beam with respect to a forward propagating reference frame. This frame is defined such that longitudinal oscillations of the field that vary as $\exp(\mathrm{i}kz)=\exp(\mathrm{i}\zeta/2\kappa)$ are factored out. It should be stressed that this factorisation is not equivalent to constraining the field to propagate along with any particular frame; the wave equation is second order in ζ and the field envelope $u(\xi,\zeta)$ may in fact contain contributions from both forward and backward propagating components.

In the paraxial approximation, the first term in Eq. (1) is neglected, whereby the NNSE reduces to the NSE. The simpler properties of the NSE make this approximation very attractive, but careful consideration of the validity of the underlying assumptions should be undertaken. The most obvious configurations for which the paraxial approximation cannot be made are those that involve input beams with significant values of κ. In free space, $\kappa=10^{-3}$, 10^{-4} and 10^{-5} imply around 10λ, 32λ and 100λ, respectively, in the full-width of the reference beam. Ultra-narrow beams can also be the result of beam evolution that involves strong

focusing stages, even when the input beam is reasonably paraxial. The signature of non-paraxiality in either of these cases is a very broad, and full, angular (spatial) spectrum. Alternatively, a beam of any width, but which is of sufficiently high intensity, can result in non-linear longitudinal phase variations that are so rapid that a full non-paraxial description is required. High intensity and beam narrowness are, however, often connected in practice; an example is the inverse relationship between peak intensity and beam width of spatial solitons. Finally, non-paraxial effects may also arise, independently of the above considerations, when two or more beams simultaneously propagate in significantly different directions. While each beam may be individually paraxial along its own propagation direction, the total angular content of the constituent beams can span a very broad spectral region.

3. Exact analytical results

A detailed account of the analytical properties of the NNSE and its soliton solutions was given in Refs. [13,14]. In this section, we briefly summarise those properties that are particularly relevant for the testing of numerical calculations. Firstly, comparison of the dispersion relation obtained for Eq. (1) and that of a discrete representation provides basic checks on the accuracy and the convergence properties of a numerical method. Secondly, conservation of the integrated light intensity can be used to test a numerical solution of the NSE, but this quantity is not conserved when the field evolves according to the non-paraxial wave equation. The integrity of solutions can, in this case, be investigated by checking whether a different conservation law is satisfied. Finally, exact analytical solutions allow one to test whether an algorithm yields meaningful results in distinct configurations of interest.

3.1. Dispersion relations

Through consideration of the plane wave solution $u(\xi,\zeta)=\sqrt{I}\exp\left[\mathrm{i}(k_\xi\xi+k_\zeta\zeta)\right]$ of the NNSE, one obtains the dispersion relation

$$\kappa k_\zeta^2+k_\zeta+\tfrac{1}{2}k_\xi^2-I=0. \tag{3}$$

It is then straightforward to show that the longitudinal wave number k_ζ can be expressed as

$$\begin{aligned}k_\zeta&=-\frac{1}{2\kappa}\pm\frac{1}{2\kappa}\sqrt{1-4\kappa\left(\frac{1}{2}k_\xi^2-I\right)}\\&=-\frac{1}{2\kappa}\pm\Delta k_\zeta,\end{aligned} \tag{4}$$

where + and − signs give solutions that represent forward and backward propagating fields, respectively. In the paraxial case, one has $k_\zeta=-(k_\xi^2/2-I)$, and propagation in only the forward direction. The corresponding dispersion curve is a parabola that simply translates along the k_ζ axis when the light intensity I is varied.

Fig. 1 shows plane wave components of non-paraxial beam propagation in linear ($I=0$) and non-linear ($I\neq 0$) media, together with a curve for paraxial propagation. The non-paraxial wave equation has dispersion curves that are ellipses in the (k_ζ,k_ξ) plane; solutions that have $k_\xi^2>2I+1/2\kappa$ correspond to evanescent waves. As the intensity increases, the size of these ellipses increases for a focusing Kerr effect, whereas it would decrease if the medium were self-defocusing. It can be seen that a wide angular spectrum (involving

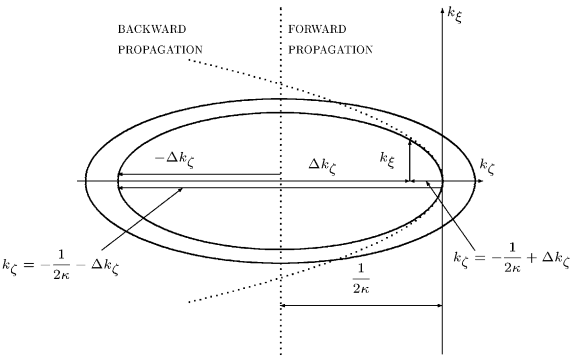

Fig. 1. Dispersion relation for the NNSE. The curve for linear propagation ($I=0$) passes through the point $(k_\zeta,k_\xi)=(0,0)$, while finite intensity ($I\neq 0$) gives a similar, but larger, ellipse. The construction of the longitudinal components of a pair of forward and backward solutions, $k_\zeta=-(1/2\kappa)\pm\Delta k_\zeta$, is detailed. The paraxial relation for linear propagation is shown (dotted) for comparison.

large $|k_\xi|$ values) gives rise to significant errors in a paraxial description of linear propagation. A forward axial component ($k_\xi = 0$) can also be susceptible to non-paraxial effects if the non-linearity is strong enough; the paraxial case yields $k_\xi = I$ for an axial component, while non-paraxiality introduces a leading order correction to this value of $-\kappa I^2$ (when $I < 1/4\kappa$).

3.2. Energy flow conservation

Any solution $u(\xi,\zeta)$ of the paraxial NSE has the property that

$$\int_{-\infty}^{+\infty} |u(\xi,\zeta)|^2 \,\mathrm{d}\xi = C, \tag{5}$$

where C is a constant. Analysis of the NNSE shows that a more general quantity replaces this invariant [14]; in non-paraxial propagation, it is the energy flow that is conserved. One finds that

$$\int_{-\infty}^{+\infty} \left(\frac{1}{2\kappa} + \frac{\partial\phi(\xi,\zeta)}{\partial\zeta}\right)|u(\xi,\zeta)|^2 \,\mathrm{d}\xi = C', \tag{6}$$

where C' is another constant and $\phi(\xi,\zeta)$ is the beam phase profile in the forward propagating reference frame, such that $u(\xi,\zeta) = |u(\xi,\zeta)| \times \exp[\mathrm{i}\phi(\xi,\zeta)]$. When the phase across the whole beam varies sufficiently slowly in the propagation direction, the paraxial conservation law is recovered. Beams for which $\kappa \to 0$ also preserve their integrated intensity, but Eq. (6) highlights the fact that this is equivalent to assuming that such beams are infinitely broad and hence have infinite energy flow.

3.3. Non-paraxial solitons

Exact analytical solutions provide an invaluable framework for systematically checking distinct regimes of application of a numerical algorithm. The absence of any solutions of this kind for non-paraxial non-linear beam evolution has been a fundamental limitation in the past. Exact bright non-paraxial soliton solutions have the form [13,14]

$$u(\xi,\zeta) = \eta\,\mathrm{sech}\left[\frac{\eta(\xi + V\zeta)}{\sqrt{1+2\kappa V^2}}\right]\exp\left[\mathrm{i}\sqrt{\frac{1+2\kappa\eta^2}{1+2\kappa V^2}} \times\left(-V\xi + \frac{\zeta}{2\kappa}\right)\right]\exp\left[\frac{-\mathrm{i}\zeta}{2\kappa}\right], \tag{7}$$

where η and V parametrise soliton amplitude and transverse velocity, respectively. Note that the forward propagating reference frame, which is implicit in the NNSE and paraxial soliton solutions, appears explicitly as the phase factor $\exp(-\mathrm{i}\zeta/2\kappa)$. Moreover, the precise conditions under which the paraxial approximation can be made may be deduced by examining this solution; the passage from the NNSE soliton to its NSE counterpart requires the multiple limit $\kappa \to 0$, $\kappa\eta^2 \to 0$ and $\kappa V^2 \to 0$. Individually, these limits specify that a beam cannot be too narrow, or too intense, or propagating at any significant angle relative to the ζ axis. The possibility of handling exact off-axis solitons is particularly interesting. In this regime, scalar theory of non-linear beam propagation can remain valid but a full non-paraxial approach is required; the NNSE also permits the analysis of several beams that propagate and interact at significant angles [12].

4. Numerical analysis

In this section, we present a study of two numerical schemes that are commonly employed in the modelling of non-linear beam propagation. Firstly, the truncation error in split-step methods is quantified and, secondly, the consequences of adopting a fully finite difference approach are examined.

4.1. Split-step methods

One of the most widely used schemes in the numerical integration of parabolic non-linear partial differential equations involves splitting the evolution operator into separate steps, that often represent the linear and non-linear operations involved. This can result in a very efficient scheme when fast Fourier transforms (FFTs) are used to implement the linear operator in the spectral do-

main. The dependence of truncation error on the step size $\Delta\zeta$, due to non-commutativity of linear and non-linear operators of the NSE, can be $O(\Delta\zeta^3)$ if each non-linear step is embedded between two linear half-steps. The Feit–Fleck non-paraxial beam propagation method [18] is based on such a scheme. Their algorithm was developed to investigate the self-focusing of 2D (transverse) beams in Kerr media. They predicted that non-paraxial effects can offset the unphysical collapse of a beam to zero transverse size that is predicted by paraxial theory. It is interesting to note that these authors state that the assumptions made in the derivation of their algorithm are not valid in the vicinity of precisely such focusing points.

We now show why conventional operator splitting strategies fail to describe accurately any sustained presence of non-paraxial effects in non-linear beam propagation, such as in the context of non-paraxial solitons. This failure is particularly striking in view of the fact that operator splitting can be done in such a way that the linear and non-linear operators individually give exact non-paraxial descriptions of diffraction and self-phase modulation (SPM), respectively. For the sake of brevity, the notation $O_{\mathrm{L}} \equiv (1/2)\partial^2/\partial\xi^2$ and $O_{\mathrm{N}} \equiv |u(\xi,\zeta)|^2$ will be used for the linear and non-linear operators of the NSE. The NNSE can then be written as

$$\frac{\partial}{\partial\zeta}u(\xi,\zeta) = \mathrm{i}\left[-\frac{1}{2\kappa} \pm \frac{1}{2\kappa}\sqrt{1+4\kappa(O_{\mathrm{L}}+O_{\mathrm{N}})}\right]u(\xi,\zeta), \tag{8}$$

where $+$ and $-$ signs correspond to solving the equation in the forward and backward ζ directions, respectively. The solution may be advanced by a forward step of length $\Delta\zeta$ through

$$u(\xi,\zeta+\Delta\zeta) \simeq \exp\left[\frac{-\mathrm{i}\Delta\zeta}{2\kappa}\left(1-\sqrt{1+4\kappa(O_{\mathrm{L}}+O_{\mathrm{N}})}\right)\right] \times u(\xi,\zeta). \tag{9}$$

This step is approximate because of a trapezoidal representation of the exponentiated integral, but otherwise the operators O_{L} and O_{N} appear in an essentially exact way. It is in this sense that the above expression can be considered as "exact". In the Feit–Fleck algorithm, the approximation $(1+4\kappa O_{\mathrm{N}})^{1/2} \simeq 1$ is employed to obtain a non-paraxial linear operator. The operators involved can also be expressed in an approximate (symmetrised) form,

$$\begin{aligned} u(\xi,\zeta+\Delta\zeta) \simeq{}& \exp\left[\frac{-\mathrm{i}\Delta\zeta}{4\kappa}\left(1-\sqrt{1+4\kappa O_{\mathrm{L}}}\right)\right] \\ &\times \exp\left[\frac{-\mathrm{i}\Delta\zeta}{2\kappa}\left(1-\sqrt{1+4\kappa O_{\mathrm{N}}}\right)\right] \\ &\times \exp\left[\frac{-\mathrm{i}\Delta\zeta}{4\kappa}\left(1-\sqrt{1+4\kappa O_{\mathrm{L}}}\right)\right] \\ &\times u(\xi,\zeta), \end{aligned} \tag{10}$$

which corresponds to a non-linear step, of size $\Delta\zeta$, sandwiched between two linear half-steps. In this representation, the exact diffraction and SPM operators for purely linear and purely non-linear non-paraxial propagation steps, respectively, are used. If normalisations (2) are used directly in the Feit–Fleck algorithm [18], as derived from the non-linear Helmholtz equation, one obtains

$$\begin{aligned} u(\xi,\zeta+\Delta\zeta) \simeq{}& \exp\left[\frac{-\mathrm{i}\Delta\zeta}{4\kappa}\left(1-\sqrt{1+4\kappa O_{\mathrm{L}}}\right)\right] \\ &\times \exp\left[\mathrm{i}\Delta\zeta O_{\mathrm{N}}\right] \\ &\times \exp\left[\frac{-\mathrm{i}\Delta\zeta}{4\kappa}\left(1-\sqrt{1+4\kappa O_{\mathrm{L}}}\right)\right] \\ &\times u(\xi,\zeta), \end{aligned} \tag{11}$$

from which Eq. (10) is recovered when the term of the non-linear Helmholtz equation that involves n_2^2 is neglected.

The accuracy of the symmetrised scheme can be ascertained by making a comparison of Eqs. (9) and (10). A power series expansion of Eq. (10) yields

$$\begin{aligned} u(\xi,\zeta+\Delta\zeta) = \{1+\mathrm{i}\Delta\zeta[(O_{\mathrm{L}}+O_{\mathrm{N}}) - \kappa(O_{\mathrm{L}}^2+O_{\mathrm{N}}^2) \\ +\cdots] + \Delta\zeta^2[-\tfrac{1}{2}(O_{\mathrm{L}}^2+O_{\mathrm{N}}^2+O_{\mathrm{L}}O_{\mathrm{N}} \\ +O_{\mathrm{N}}O_{\mathrm{L}})+\cdots]+\cdots\}u(\xi,\zeta), \end{aligned} \tag{12}$$

where at each power of the step size, there is an infinite series of terms arising from successive powers of κ. The truncation error involved can be

quantified if Eq. (9) is also expanded in a power series. This gives

$$u(\xi,\zeta+\Delta\zeta) = \{1 + \mathrm{i}\Delta\zeta[(O_\mathrm{L}+O_\mathrm{N}) - \kappa(O_\mathrm{L}+O_\mathrm{N})^2 + \cdots] + \Delta\zeta^2[-\tfrac{1}{2}(O_\mathrm{L}+O_\mathrm{N})^2 + \kappa(O_\mathrm{L}+O_\mathrm{N})^3 + \cdots] + \cdots\}u(\xi,\zeta). \quad (13)$$

The error is found by simply examining the difference of Eqs. (12) and (13). For example, the $O(\Delta\zeta)$ error terms are

$$E_1 = \mathrm{i}\Delta\zeta[-\kappa(O_\mathrm{L}O_\mathrm{N}+O_\mathrm{N}O_\mathrm{L}) + 2\kappa^2(O_\mathrm{L}^2O_\mathrm{N} + O_\mathrm{L}O_\mathrm{N}O_\mathrm{L} + O_\mathrm{L}O_\mathrm{N}^2 + O_\mathrm{N}^2O_\mathrm{L} + O_\mathrm{N}O_\mathrm{L}O_\mathrm{N} + O_\mathrm{N}O_\mathrm{L}^2) + \cdots]u(\xi,\zeta). \quad (14)$$

Thus, while a symmetrised split-step algorithm for the paraxial NSE yields a truncation error of $O(\Delta\zeta^3)$, the corresponding scheme for non-paraxial propagation leads to a much larger error of $O(\Delta\zeta)$.

4.2. Finite difference methods

In contrast to the above split-step scheme, a finite difference approach involves solving both the linear and non-linear parts of the NNSE simultaneously. This is made possible by approximating each differential operator with an appropriate finite difference formula. The truncation error that results depends on the transversal grid resolution $\Delta\xi$ and can, in principle, be made as small as desired. Use of a popular three-point approximation for the second order transverse derivative gives the result

$$\frac{\partial^2 u(\xi,\zeta)}{\partial\xi^2} = \frac{u(\xi+\Delta\xi,\zeta) - 2u(\xi,\zeta) + u(\xi-\Delta\xi,\zeta)}{\Delta\xi^2} - \frac{1}{12}\Delta\xi^2\frac{\partial^4 u(\xi,\zeta)}{\partial\xi^4} + \cdots \quad (15)$$

The first term on the right-hand side of Eq. (15) is the finite difference approximation of the derivative and the second term can be used to estimate the error in this approximation. The leading order error term is proportional to $\Delta\xi^2$, which suggests that a moderate number of transverse data points could make this error relatively small. However, the non-paraxial soliton solution has $|\partial^4 u(\xi,\zeta)/\partial\xi^4|$ proportional to V^4 and the actual number of data points, required for a reasonable level of accuracy, rapidly becomes prohibitive as V is increased. If a higher order finite difference approximation is used, instead of a three-point formula, the error term will involve, not only a higher power of $\Delta\xi$ but also, a higher order partial derivative. This implies an even higher power of V and, again, an extremely high number of transverse data points for accurate calculations. A similar argument can be presented for any non-paraxial beam that involves a wide angular range of spectral components.

5. New numerical algorithms

5.1. Modified split-step method

The magnitude of the error in the symmetrised split-step solution of the NNSE depends on both the computational and the physical parameters considered. We now show that one can often identify the most significant error terms and introduce appropriate corrections to the numerical scheme to eliminate them. To demonstrate this approach, we focus on the generation and the evolution of non-paraxial bright soliton solutions when non-paraxial effects arise fundamentally from the angle θ between the light beam and the ζ axis.

For this configuration, we consider $\eta \simeq 1$, $\kappa \ll 1$ and allow $\tan^2\theta = 2\kappa V^2$ to take arbitrarily large values. Substitution of the soliton solution into the equation for E_1 reveals that the most significant error terms arise from the fact that $(O_\mathrm{L})^n u(\xi,\zeta)$ is proportional to $(V^2)^n$. At each power m of κ, a number of operators of the form $O_\mathrm{N}O_\mathrm{L}^m$ can be identified. The error introduced by these operators has a magnitude of the order $\Delta\zeta(\kappa V^2)^m$ which generally cannot be neglected. One can also show that any remaining terms in the error expression are much smaller than this, for any value of m.

A modified version of the split-step approach can be proposed that deals with the large truncation errors that arise from off-axis non-paraxiality.

We choose a specific objective of finding a modified non-linear operator that leads to a negligible first order error term. Since we are concerned with solutions that have $\eta \simeq 1$, the exact operator for a purely non-linear step can be approximated using

$$-\frac{\mathrm{i}}{2\kappa}\left(1-\sqrt{1+4\kappa O_{\mathrm{N}}}\right) \simeq \mathrm{i}O_{\mathrm{N}}. \tag{16}$$

Hence, the equation describing non-paraxial SPM,

$$\kappa\frac{\partial^2 u}{\partial\zeta^2}+\mathrm{i}\frac{\partial u}{\partial\zeta}+O_{\mathrm{N}}u=0, \tag{17}$$

is given to a first approximation by the corresponding paraxial equation:

$$\mathrm{i}\frac{\partial u}{\partial\zeta}+O_{\mathrm{N}}u=0. \tag{18}$$

The linear operator O_{L} is now introduced into this approximation by proposing a new generalised form of the non-linear operator,

$$\mathrm{i}\frac{\partial u}{\partial\zeta}+O_{\mathrm{N}}[1+f(O_{\mathrm{L}};\kappa)]u=0, \tag{19}$$

where $f(O_{\mathrm{L}};\kappa)$ is, at this stage, an undetermined function of the operator O_{L} and the non-paraxial parameter κ. The precise form of this function is obtained by stipulating that significant $O(\Delta\zeta)$ error terms are cancelled up to a given order of κ, whereby one finds that

$$f(O_{\mathrm{L}};\kappa) = -2\kappa O_{\mathrm{L}}+6\kappa^2 O_{\mathrm{L}}^2-20\kappa^3 O_{\mathrm{L}}^3 + 70\kappa^4 O_{\mathrm{L}}^4-252\kappa^5 O_{\mathrm{L}}^5+924\kappa^6 O_{\mathrm{L}}^6+\cdots \tag{20}$$

The accuracy of the resulting modified split-step method can be verified by comparison of numerical and analytical solutions. Fig. 2 shows numerical results for an initial condition that corresponds to a non-paraxial soliton with $\kappa = 0.001$ and $V = 10$. A curve of peak amplitude $|u|_m$ versus propagation distance should be a straight horizontal line for this boundary condition. The numerical solution given by the Feit–Fleck method is found to exhibit large oscillations as the beam propagates. Three curves are also shown for the modified split-step method where an increasing number of correction terms are included in $f(O_{\mathrm{L}};\kappa)$; the first curve takes only the first term in Eq. (20) into account, while the other two curves include terms in κ^2 and κ^3. Excellent convergence to the desired solution is found as higher orders of κ are included in the modified non-linear operator. In particular, with only three correction terms, the numerical solution always has $|u|_m$ within 0.5% of its exact value of unity. Furthermore, calculation of the energy flow implied by each set of data shows convergence to a constant value as the number of correction terms is increased.

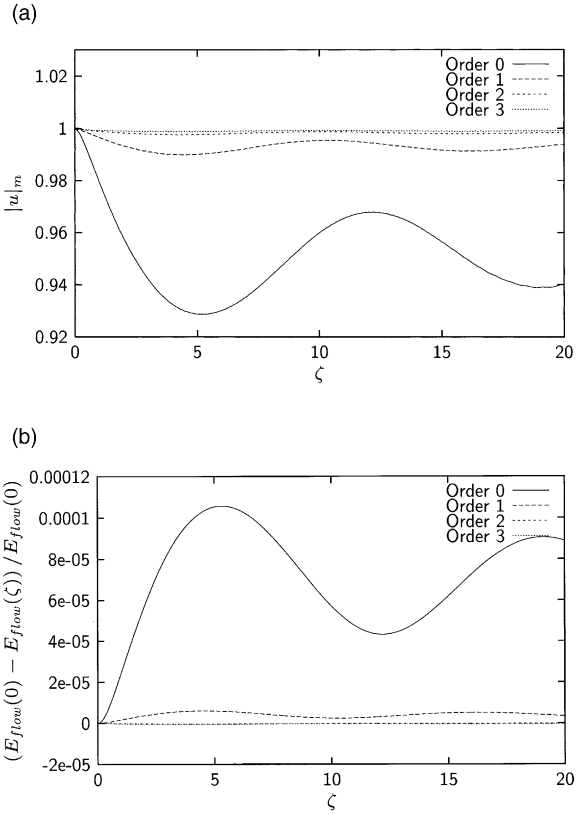

Fig. 2. Evolution of (a) the peak beam amplitude $|u|_m$ and (b) the energy flow E_{flow} for an exact non-paraxial soliton initial condition with $\eta = 1$, $V = 10$ and $\kappa = 0.001$. The curve labelled "order 0" was calculated using the Feit–Fleck method, while curves labelled "orders 1, 2 and 3" were generated using the modified split-step method with one, two and three correction terms, respectively.

5.2. Difference-differential equation method

The modified split-step approach has clear advantages over conventional non-paraxial beam

propagation methods in terms of both accuracy, when compared with the Feit–Fleck method, and efficiency, when compared with fully finite difference schemes. However, the choice of which error terms to eliminate varies when the specific character of the non-paraxiality is changed. The approach thus suffers from the limitation that no one formulation can accurately model all possible configurations. We note that a similar conclusion may also be drawn concerning more general model equations for non-paraxial beam evolution whose derivation relies on an order-of-magnitude analysis [17]. We have thus derived an additional algorithm that has wider applicability. In this alternative method, we employ finite difference formulae to approximate derivatives with respect to the ζ coordinate but, in view of the difficulties resulting from a finite difference representation of the transverse derivative, the diffraction operator is implemented in the spectral domain. The finite difference formulae we have used for the second and first order ζ derivatives are

$$\left[\frac{\partial^2 u(\xi,\zeta)}{\partial\zeta^2}\right]_{\zeta=n\,\Delta\zeta} = \frac{u_{n+1}(\xi) - 2u_n(\xi) + u_{n-1}(\xi)}{\Delta\zeta^2} + O(\Delta\zeta^2) \tag{21}$$

and

$$\left[\frac{\partial u(\xi,\zeta)}{\partial\zeta}\right]_{\zeta=n\,\Delta\zeta} = \frac{u_{n+1}(\xi) - u_{n-1}(\xi)}{2\,\Delta\zeta} + O(\Delta\zeta^2), \tag{22}$$

where $u_n(\xi) \equiv u(\xi, n\,\Delta\zeta)$. Substitution of these formulae in the NNSE yields the difference-differential equation

$$u_{n+1}(\xi) = \frac{1}{(2\kappa + \mathrm{i}\,\Delta\zeta)}\left[\left(4\kappa - \Delta\zeta^2\frac{\partial^2}{\partial\xi^2} - 2\,\Delta\zeta^2|u_n(\xi)|^2\right)u_n(\xi) - (2\kappa - \mathrm{i}\,\Delta\zeta)u_{n-1}(\xi)\right].$$

This equation defines an explicit algorithm in which the effect of the transverse differential operator $\partial^2/\partial\xi^2$ can be computed efficiently using FFTs. The accuracy and convergence properties of this method are analysed by deriving a numerical dispersion relation. Considering plane wave components at discrete values of ζ,

$$u_n(\xi) = \sqrt{I}\exp\left[\mathrm{i}(nk_\zeta\,\Delta\zeta + k_\xi\xi)\right] \tag{23}$$

yields the numerical dispersion relation

$$k_\zeta(k_\xi) = \pm\frac{1}{\Delta\zeta}\cos^{-1}\left[\frac{\frac{1}{2\kappa} + \left(\frac{\Delta\zeta}{2\kappa}\right)^2\left(\frac{1}{2}k_\xi^2 - I\right)}{\frac{1}{2\kappa}\sqrt{1 + \left(\frac{\Delta\zeta}{2\kappa}\right)^2}}\right] - \frac{1}{\Delta\zeta}\tan^{-1}\left(\frac{\Delta\zeta}{2\kappa}\right). \tag{24}$$

A comparison with the dispersion relation of the partial differential equation, Eq. (4), reveals the same functional dependence with respect to transverse wave number and intensity of the form $k_\xi^2/2 - I$. The appearance of this form expresses the trade-off between on- and off-axis components of the total wave vector and that a non-linear contribution is made to this latter quantity by the Kerr effect. The numerical dispersion relation is plotted in Fig. 3 for a range of longitudinal step sizes. A curve for the exact dispersion relation is also plotted and a fast convergence of the numerical method is demonstrated as $\Delta\zeta/\kappa \to 0$. The requirement that the argument of the $\cos^{-1}$ term in Eq. (24) be less than unity yields the correct physical upper limit on the magnitude of the transverse wave number, through

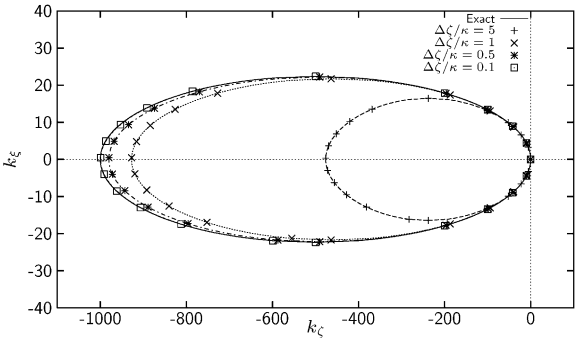

Fig. 3. Numerical dispersion relation for the difference-differential equation method when $I = 0$. A rapid convergence to the corresponding exact (NNSE) curve is demonstrated as the step size $\Delta\zeta$ is reduced ($\Delta\zeta/\kappa \to 0$).

$$\lim_{\Delta\zeta/\kappa\to 0}\left(k_\xi^2\right)_{\max} = 2I + \frac{1}{2\kappa}, \tag{25}$$

and also that convergence of the numerical dispersion relation requires $\Delta\zeta \ll \kappa$. In terms of unscaled variables, this latter condition corresponds to $\Delta z \ll \lambda$, which is an expected result for non-paraxial propagation.

The difference-differential algorithm has the advantage of being explicit, which permits a simple implementation and low computation load in the solution of the NNSE. In common with solving second order differential equations analytically, the numerical method requires two boundary conditions to define a particular solution. The transverse field envelope may, for example, be specified at $\zeta = 0$ and at $\zeta = \Delta\zeta$. If the initial stages of beam evolution are sufficiently paraxial, $u(\xi, \Delta\zeta)$ can be calculated using the Feit–Fleck method. Otherwise, the modified split-step method can be used to find the field at $\zeta = \Delta\zeta$. An alternative set of boundary conditions would be the field profile and its longitudinal derivative at $\zeta = 0$.

The dispersion curves shown in Fig. 3 correspond to cases where the longitudinal wave number k_ζ is real. It may seem that circumstances when k_ζ becomes complex are not of any interest, since this implies attenuation of a field. A key point to note is that one solves the NNSE in only one longitudinal direction and that the resulting solution can contain contributions from both forward- and backward-travelling waves. A backward field that is decaying exponentially can appear in the solution as the exponential growth of a small seed in the forward direction. This potential problem can be overcome by filtering out both forward and backward evanescent components in the numerical solution. This is achieved by removing any contributions to the solution that have spectral components with

$$k_\xi^2 > \frac{4\kappa}{\Delta\zeta^2}\left[\sqrt{1+\left(\frac{\Delta\zeta}{2\kappa}\right)^2} - 1\right]. \tag{26}$$

Since evanescent components should rapidly die out during beam evolution, one expects that their removal from the numerical solution will not result in any undesirable effects. We have checked that such filtering can indeed be performed without affecting conservation of the energy flow or the integrity of an exact solution, even when large k_ξ^2 values are involved.

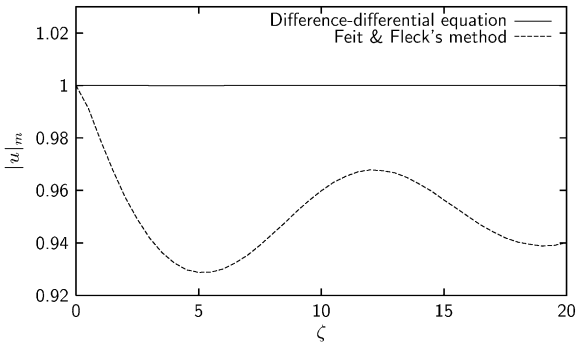

Fig. 4. Evolution of the peak value of $|u(\xi,\zeta)|$, for exact non-paraxial soliton ($\kappa = 0.001$, $V = 10$) initial conditions, obtained from the difference-differential equation method (—) and Feit–Fleck method (- - -).

Our first demonstration of the difference-differential equation method concerns the propagation of an exact non-paraxial soliton solution (7). Fig. 4 shows the evolution of the peak value of $|u(\xi,\zeta)|$ for initial conditions corresponding to a non-paraxial soliton with $\kappa = 0.001$ and $V = 10$. Whereas the results calculated by means of the difference-differential equation (solid line) show the expected constant value for an exact solution, those obtained from Feit–Fleck method (dashed line) display oscillations. Such oscillations lead to the formation of a bright soliton which is the asymptotic exact solution of the model described by the split-step equations and this solution differs from that derived from the NNSE. A detailed study of the re-shaping of beams towards non-paraxial solitons was presented in Ref. [14].

For a second application of the difference-differential equation method, the role of an additional transverse derivative in the NNSE is investigated. Eq. (1) then takes the form

$$\kappa\frac{\partial^2 u}{\partial\zeta^2} + \mathrm{i}\frac{\partial u}{\partial\zeta} + \frac{1}{2}\left(\frac{\partial^2 u}{\partial\xi^2} + \frac{\partial^2 u}{\partial\psi^2}\right) + |u|^2 u = 0, \tag{27}$$

and no exact analytical non-linear beam solutions are known. To allow a comparison with previous work, we choose the same parameters as those

used in Fig. 1 of Ref. [17]. Their units are similar to ours, except that the width of their reference Gaussian beam is $w = w_0/2$; this makes our parameter κ equivalent to their $\sigma_0^2/2$. We consider an input beam with Gaussian cross-section and planar transverse phase profile, $u(\xi,\psi,0) = u_0 \exp[-(\xi^2+\psi^2)]$, with $u_0 = 1.4575$ and $\kappa = 2.43 \times 10^{-3}$ [17]. A transverse grid with 256×256 points and a step size of $\Delta\zeta = 10^{-4}$ proves to be sufficient for an accurate calculation of the solution.

Fig. 5(a) shows the evolution of normalised peak intensity $|u(0,\zeta)|^2/|u(0,0)|^2$ with respect to ζ, as predicted by paraxial theory, by the Feit–Fleck method, and by the difference-differential equation method. It is well known that the paraxial approximation leads to an unphysical collapse of the solution to zero transverse size. The other two methods predict the elimination of this uncontrolled focusing, but it is clear that they also give quantitatively different results. The results obtained by means of the Feit–Fleck method display a staircase-like behaviour of the paraxial invariant with sudden drops near the focusing points [18] and almost constant values elsewhere. There are also relatively large changes in the calculated non-paraxial invariant in the vicinity of the same points, as shown in Fig. 5(b). In part (c) of Fig. 5, the conserved quantities of paraxial and non-paraxial propagation are plotted using the data from the difference-differential equation method. It is found that the energy flow is conserved to within

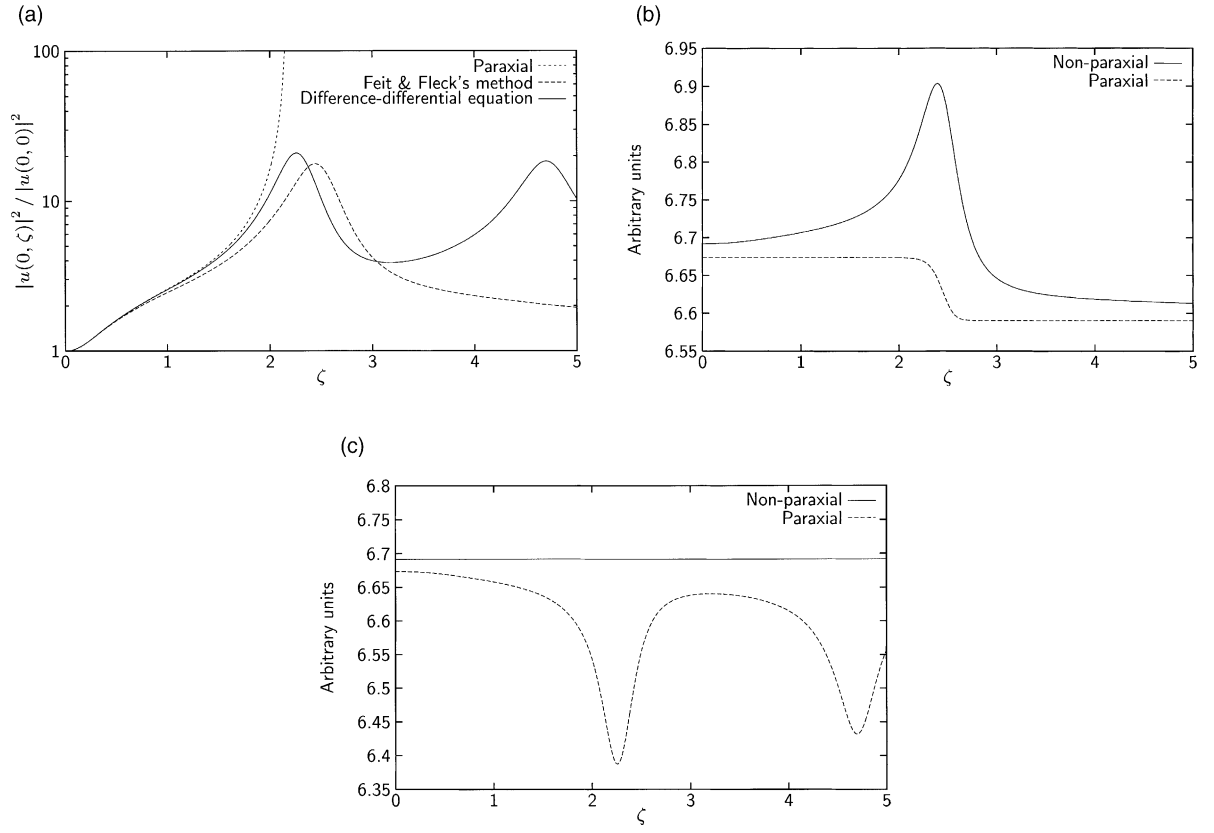

Fig. 5. 2D (transverse) self-focusing arising from Gaussian beam input with peak amplitude $u_0 = 1.4575$ and $\kappa = 2.43 \times 10^{-3}$. (a) Curves of normalised peak intensity, as predicted by paraxial theory (···), the Feit–Fleck method (- - -) and the difference-differential equation method (—). Comparison of the paraxial and non-paraxial propagation invariants according to the results obtained with the Feit–Fleck method (b) and the difference-differential equation method (c).

one part in 10^6, while the paraxial invariant shows relatively large deviations in regions where the beam focuses down to a small spot. This proves that the results obtained by means of the difference-differential equation are consistent with the analytical properties of the NNSE.

5.3. Performance evaluation

In order to evaluate the performance of the proposed numerical schemes, we present results of the required CPU time per propagation step for each of the methods described in Sections 4.1 and 4.2, along with results for the Feit–Fleck algorithm. The data reported in this section has been obtained using a PC compatible desktop computer equipped with an AMD K6 processor running at 350 MHz and 64 MB of RAM memory. We have used Octave under Linux for the computations. Fig. 6 shows the CPU time for one propagation step of the $(1+1)$D problem as a function of the number of grid points N in the transverse dimension. While the CPU time required by the difference-differential equation method is close to that of the Feit–Fleck algorithm, the corresponding time for one iteration of the modified split-step method is approximately twice that value.

These results can be explained in terms of the number of important operations involved, i.e. how many FFTs, complex multiplications and complex exponentials are needed for each step. The basic structure of the calculations for both the Feit–Fleck and the modified split-step methods is the symmetrised form of Eq. (11) where Eq. (19) has been used for the non-linear step in the modified split-step method. The computations of the linear operators involve four FFTs and, for the modified non-linear step, a predictor–corrector scheme has also been implemented that requires and additional four FFTs. Thus, the modified split-step method requires twice the number of FFTs of the Feit–Fleck algorithm and this factor dictates the overall CPU time. The full propagation step in the difference-differential equation method requires two FFTs and another two are used to filter out evanescent components of the field at each propagation step, resulting in the same number of FFTs as the Feit–Fleck scheme; while no complex exponentials are evaluated, a larger number of complex multiplications than the Feit–Fleck method are involved. A key point to recall is that the CPU time per step can be reduced in both the Feit–Fleck method and the modified split step when output data is not required after each step. In that case, each second linear half-step can be combined with the first linear half-step of the next stage resulting in a reduction of two FFTs and N complex multiplications per step.

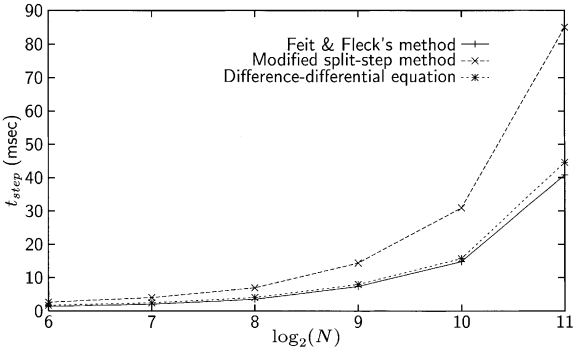

Fig. 6. CPU time (in milliseconds) for one step of the Feit–Fleck, the modified split step and the difference-differential equation methods using a desktop computer.

6. Conclusions

Exact analytical results have been employed in the development and testing of two novel non-paraxial beam propagation methods. A modified split-step method and a difference-differential equation method were described and analysed, and their predictions have been rigorously verified. Our goal has been to demonstrate, for the first time, how to model accurately the interplay between Kerr self-focusing and both longitudinal and transverse linear diffraction of beams; this has been a long-standing problem.

The scalar framework adopted permitted testing of numerical data using recent analytical results. This framework is valid in some situations, such as when non-paraxiality arises from the oblique propagation or interaction of beams, but may be incomplete during axial self-focusing when vectorial effects also come into play. Most importantly,

this work provides the foundations upon which further investigations may be based; the modelling of numerous higher order effects and different physical geometries can now be undertaken with much greater confidence. We believe that the difference-differential approach will prove to be flexible in the accommodation of additional effects, such as those listed at the end of Section 1. However, a thorough account of the properties of the generalised difference-differential equation(s) that arise when particular higher order effects are included is outwith the scope of this paper.

Acknowledgements

This project was supported, in part, by Junta de Castilla y León project number VA16/99 and EPSRC grant GR/L90583.

References

[1] G.S. McDonald, W.J. Firth, J. Mod. Opt. 37 (1990) 613.
[2] G.S. McDonald, W.J. Firth, J. Opt. Soc. Am. B 7 (1990) 1328.
[3] G.S. McDonald, W.J. Firth, J. Opt. Soc. Am. B 10 (1993) 1081.
[4] W.J. Firth, A.J. Scroggie, Phys. Rev. Lett. 76 (1996) 1623.
[5] M. Brambilla, L.A. Lugiato, F. Prati, L. Spinelli, W.J. Firth, Phys. Rev. Lett. 79 (1997) 2042.
[6] W.J. Firth, G.K. Harkness, Asian J. Phys. 7 (1998) 665.
[7] L. Spinelli, G. Tissoni, M. Brambilla, F. Prati, L.A. Lugiato, Phys. Rev. A 58 (1998) 2542.
[8] L. Spinelli, M. Brambilla, Euro. Phys. J. D 6 (1999) 523.
[9] G. Tissoni, L. Spinelli, M. Brambilla, T. Maggipinto, I.M. Perrini, L.A. Lugiato, J. Opt. Soc. Am. B 16 (1999) 2083.
[10] G. Tissoni, L. Spinelli, M. Brambilla, T. Maggipinto, I.M. Perrini, L.A. Lugiato, J. Opt. Soc. Am. B 16 (1999) 2095.
[11] L.A. Lugiato, L. Spinelli, G. Tissoni, M. Brambilla, J. Opt. B – Quant. Semi. Opt. 1 (1999) 43.
[12] P.D. Miller, N.N. Akhmediev, Phys. Rev. E 53 (1996) 4098.
[13] P. Chamorro-Posada, G.S. McDonald, G.H.C. New, J. Mod. Opt. 45 (1998) 1111.
[14] P. Chamorro-Posada, G.S. McDonald, G.H.C. New, J. Mod. Opt. 47 (2000) 1877.
[15] N. Akhmediev, A. Ankiewicz, J.M. Soto-Crespo, Opt. Lett. 18 (1993) 411.
[16] J.M. Soto-Crespo, N. Akhmediev, Opt. Commun. 101 (1993) 223.
[17] S. Chi, Q. Guo, Opt. Lett. 20 (1995) 1598.
[18] M.D. Feit, J.A. Fleck, J. Opt. Soc. Am. B 7 (1988) 633.
[19] V.V. Afanasjev, J.S. Aitchison, Y.S. Kivshar, Opt. Commun. 116 (1995) 331.
[20] P. Chamorro-Posada, G.S. McDonald, G.H.C. New, F.J. Fraile-Pelaez, IEEE Trans. Magn. 35 (1999) 1558.
[21] Yu.M. Aliev, A.D. Boardman, A.I. Smirnov, K. Xie, A.A. Zharov, Phys. Rev. A 53 (1996) 5409.
[22] J. Scheuer, M. Orenstein, Opt. Lett. 24 (1999) 1735.
[23] A.D. Boardman, K. Marinov, D.I. Pushkarov, A. Shivarova, Opt. Quant. Electron. 32 (2000) 49.